Two-dimensional model for femtosecond pulse conversion and compression using high-order stimulated Raman scattering in solid hydrogen

Nguyen Hong Shon,* Fam Le Kien,† and K. Hakuta
Department of Applied Physics and Chemistry, University of Electro-Communications, Chofu, Tokyo 182-8585 Japan and CREST, Japan Science Technology Corporation, Chofu, Tokyo 182-8585 Japan

A. V. Sokolov
Department of Physics and Institute for Quantum Studies, Texas A&M University, College Station, Texas 77843-4242
(Received 11 September 2001; published 7 February 2002)

We present a numerical model for the interaction of a femtosecond probe pulse with a Raman medium excited by two nanosecond laser pulses in solid hydrogen. The model consists of a solution of a system of Bloch equations (for the medium state) and of the two-dimensional wave equation (for the field propagation). It is shown that by optimizing the tilt angle between the two driving pulses and the interaction length, the power of the probe pulse can be converted either into a quasicontinuous broadband spectrum or into a selected high-order sideband. The first situation can be used for generation of subfemtosecond pulses. The second situation can be used for the wavelength conversion of a femtosecond probe pulse from the infrared to the ultraviolet region. Due to the transfer of energy from the driving pulses, the energy conversion efficiency of these processes (with respect to the probe pulse) can be larger than unity.

DOI: 10.1103/PhysRevA.65.033809 PACS number(s): 42.65.Re, 32.80.Qk, 42.50.Gy, 42.65.Sf

I. INTRODUCTION

The generation of subfemtosecond pulses (SFPs) is of great importance for various applications in science and technology. This is a challenging problem and has been attracting much attention (see, for example, Ref. [1]). The basis of all traditional pulse compression schemes is the interplay between the Kerr-induced self-phase modulation and the negative group-velocity dispersion (GVD). In this way, the shortest pulses achieved today (~ 4.5 fs) approach the duration of the optical cycle ($\simeq 2.7$ fs for Ti:sapphire laser) and are limited by the accessible bandwidth. To go beyond the 1 fs barrier different methods have been proposed. One of the promising methods is high-harmonic generation (HHG) with an intense, few-cycle Ti:sapphire laser pulse in noble gases [1–3]. It has been predicted that the pulse composed of consecutive harmonics would have the duration which is shorter than 1 fs. The latest development in this area is the experimental demonstration of subfemtosecond pulse structure [4,5]. The most serious disadvantage of the HHG method is the low-energy conversion efficiency ($\leqslant 10^{-3}$). Another method is high-order stimulated Raman scattering (SRS) [6–12]. The key idea of this method is the use of a broad Raman spectrum for the pulse compression. For example, Yoshikawa and Imasaka suggested the use of phase-locked Raman lines for short-pulse generation [6]. Kaplan predicted 2π Raman solitons with phase-locked spectrum [7]. Harris and Sokolov proposed to use two single-mode laser beams for an adiabatic molecular excitation [8]. Nazarkin *et al.* and Belenov *et al.* suggested the use of an impulsive excitation technique [9,10]. Kalosha and Herrmann proposed the use of subpicosecond pumping followed by external phase compensation [12]. The most important advantage of the SRS method is the high-energy conversion efficiency (near-complete conversion can be achieved). A disadvantage is that it leads to trains of many pulses. It is important to note that the SFPs generated by the SRS method usually consist of single or a half an oscillation and represent a special type of radiation (a pulse without a carrier frequency [9,10,13]). Such pulses, which in the past have only been available in the tetrahertz spectral region (see, for example [14]), can bring interesting physical phenomena in the light-matter interaction and enrich the potential applications for ultrashort pulses.

In our previous paper [15] we have proposed a SRS technique for the SFP generation: a femtosecond (fs) probe pulse beats (instantaneously) with a Raman coherence adiabatically prepared by two nanosecond (ns) driving pulses in solid hydrogen (H_2). This technique combines the advantage of the cw two-color laser pumping [8] in producing large coherence and the advantage of the short-pulse excitation [12] in reducing the number of generated SFPs. It also utilizes the advantage of solid H_2 as a Raman medium with high-molecule density, short-medium length, small dephasing rate, and negligible phase mismatch [16–18]. By numerical modeling for solid H_2, we have shown that the beating of a fs pulse with a driven Raman coherence can generate a doublet or triplet of pulses with a pulse length of 0.5 fs without the need for external phase compensation. In that paper, we have used the one-dimensional (1D) numerical model which is applicable along the assumptions that pump and probe pulses are applied collinearly and have infinite beam sizes (the laser intensity distribution is uniform across the propagation direction). We have also assumed that the Raman generation occurs in the same direction, which we justified by the fact that

*Permanent address: Institute for Nuclear Sciences and Technique, Hanoi, Vietnam.

†Permanent address: Department of Physics, University of Hanoi, Hanoi, Vietnam.

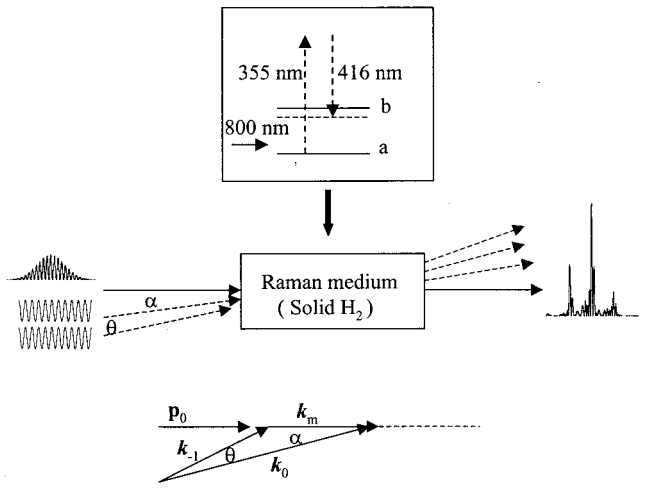

FIG. 1. Schematic of the technique. $\mathbf{k}_0$, $\mathbf{k}_{-1}$, $\mathbf{p}_0$, and $\mathbf{k}_m$ are wave vectors of two nanosecond driving pulses, femtosecond probe pulse, and generated Raman coherence. The θ is the tilt angle between two ns driving pulses. The α is the angle between generated Raman coherence and pump pulse. The beating of the probe pulse with the Raman coherence occurs along the wave vector $\mathbf{k}_m$.

dispersion plays a negligible role in the high-coherence regime.

A real experimental picture can be far richer than the 1D theory. An experiment with a two-frequency pump has confirmed that in a low-pressure gas multiple sideband generation can occur collinearly; however, at a higher pressure (higher dispersion), for the same pump parameters the anti-Stokes generation is less efficient and forms ring structures (see Fig. 2(d) of Ref. [19]). In earlier experiments with solid H_2 Hakuta *et al.* [16] have shown simultaneous generation of the ring and on-axis components. It is also of interest to consider a situation where laser beams are not collinear: by varying the angles among the applied beams one can control the magnitude and the direction of the wave vector for the Raman coherence, and at the same time achieve beam separation at the output.

The present paper extends our previous theoretical investigations to the two-dimensional (2D) case. The 2D model enables us to consider the noncollinear beam propagation geometry (see Fig. 1) and to take into account the realistic intensity profiles and diffraction effects. We use our model to investigate the interaction of a fs probe pulse with a Raman medium excited by two ns laser pulses. In this paper (i) we verify the results obtained under the 1D assumption (subfemtosecond pulse generation in solid H_2 as described in Ref. [15]); and (ii) we use the 2D model to study a regime, which is not accessible to 1D models, and show the possibility for a noncollinear selective sideband conversion. To the best of our knowledge, this is the first time the 2D numerical model has been used to study multisideband Raman generation. We shall show that by optimizing the tilt angle between two driving pulses and the interaction length, the power of a fs probe pulse can be converted either into a quasicontinuous broadband spectrum or into a selected high-order sideband. The first situation can be used for generation of SFPs. The second situation can be used for wavelength conversion of a fs probe pulse from infrared (IR) to ultraviolet (UV) region.

II. NUMERICAL MODEL

In this paper we consider the interaction of a fs probe pulse with a Raman medium (solid H_2) excited by two ns laser pulses. The ns pulses are tuned close to the Raman transition $|a\rangle \rightarrow |b\rangle$, but far detuned from the upper electronic states $|j\rangle$ of the molecules. This far-off resonance regime permits adiabatic preparation of a large Raman coherence [8,17,18]. The probe pulse has a duration which is comparable to the Raman period (~ 8 fs) and has an energy that is much smaller than the energy of driving pulses. Therefore the influence of the probe pulse on the medium state (via impulsive SRS or Kerr effect) is negligible. Our simulations consist of two steps which occur on two significantly different time scales.

The first step, the ''coherence preparation,'' occurs on the ns time scale. In this regime the calculations are carried out in frequency domain based on the slowly varying envelope approximation (SVEA). This approach is accurate when the durations of driving pulses are much longer than the Raman period. The basic equations for 1D calculations in this regime have been derived in papers [7,8,11]. The generalization of the formalism for the 2D case is as follows. We consider the propagation of waves in 2D xz plane (electric fields of waves are perpendicular to this plane). We assume that the waves propagate primarily along the z axis and the variations of wave envelopes in z direction change slowly compared not only to $\exp(ikz)$ but also to the variation in transverse direction x (the paraxial approximation). Further, we make the SVEA, i.e., we assume that wave envelopes vary slowly in time compared to $\exp(-i\omega t)$. Then the total electric field can be expressed as a sum of the Raman sideband fields

$$E(x,z,t)=\frac{1}{2}\sum_q E_q(x,z,t)\exp(ik_q z-\omega_q t)+\text{c.c.}, \quad (1)$$

where q is the numeration of sideband fields, $k_q=\omega_q/c$; $\omega_q=\omega_0+q(\omega_b-\omega_a-\delta)=\omega_0+q\omega_m$; δ is the two-photon detuning; ω_0 and ω_{-1} are the frequencies of two driving pulses; ω_a, ω_b, and ω_m are the energy of levels a and b and modulation frequency, respectively. It is important to note that the paraxial approximation, which is valid for beam sizes much larger than the wavelength, does not impose any limitation on the pulse duration [20]. The expression (1) does not mean waves propagate strictly along the z axis. The actual propagation direction of each Raman sideband is defined by the phase factor of their wave envelope $E_q(x,z,t)$. Changing to the local time ($\tau=t-z/c$) and performing the same procedures as described in [8,11] we obtain the Bloch equations for density-matrix elements ρ_{aa}, ρ_{bb}, and ρ_{ab} and the wave equation for wave envelopes

$$\left(\frac{\partial}{\partial\tau}+\frac{1}{T_2}-i\delta\right)\rho_{ab}=i(\Omega_{aa}-\Omega_{bb})\rho_{ab}+i\Omega_{ab}w,$$

$$\frac{\partial w}{\partial \tau}+\frac{w+1}{T_1}=2i(\Omega_{ab}^{*}\rho_{ab}-\Omega_{ab}\rho_{ab}^{*}), \tag{2}$$

$$\left(\frac{\partial^2}{\partial x^2}+2ik_q\frac{\partial}{\partial z}\right)E_q=-\frac{2N\hbar\omega_q^2}{\epsilon_0 c^2}[(a_q\rho_{aa}+b_q\rho_{bb})E_q + d_{q-1}\rho_{ab}^{*}E_{q-1}+d_q\rho_{ab}E_{q+1}], \tag{3}$$

where $w=\rho_{bb}-\rho_{aa}$ is the population difference; T_1 and T_2 are the population decay and dephasing times; Ω_{aa}, Ω_{bb}, and Ω_{ab} are the Stark shifts and the two-photon Rabi frequency, respectively. The expressions for coupling coefficients a_q, b_q, and d_q and the other parameters are given in Ref. [11].

The second step, the ''beating'' of the prepared Raman coherence with a fs probe pulse, occurs on the fs time scale. In this regime, the paraxial approximation is valid. However, since the duration of the probe pulse is comparable to the optical period, the SVEA is not applicable. The electric field $F(x,z,\tau)$ of the fs probe pulse should be expressed by the exact Fourier integral as follows:

$$F(x,z,\tau)=\frac{1}{2}\int_{-\infty}^{\infty}F(x,z,\omega)e^{-i\omega\tau}d\omega. \tag{4}$$

Performing similar procedures as in the above equation one gets the wave equation for the probe pulse field

$$\left(\frac{\partial^2}{\partial x^2}+2ik_\omega\frac{\partial}{\partial z}\right)F(x,z,\omega) = -\frac{2N\hbar\omega^2}{\epsilon_0 c^2}[(a_\omega\rho_{aa}+b_\omega\rho_{bb})F(x,z,\omega) + d_{\omega-\omega_m}\rho_{ab}^{*}F(x,z,\omega-\omega_m)+d_\omega\rho_{ab}F(x,z,\omega+\omega_m)], \tag{5}$$

where $k_\omega=\omega/c$; a_ω, b_ω, and d_ω are the coefficients a_q, b_q, and d_q evaluated at $\omega_q=\omega$. The structures of Eqs. (3) and (5) are the same. The only difference is that the first one is used for a discrete function and the second one is used for a continuous function in the frequency domain. The set of Eqs. (2), (3), and (5) are central equations of our model. As mentioned above, we shall consider the case of the probe pulse with an energy many orders of magnitude less than the energy of driving pulses. The influence of the probe pulse on the medium state and on the Stark shifts and the two-photon Rabi frequency is negligible. Therefore, the density-matrix elements ρ_{aa}, ρ_{bb}, and ρ_{ab} in Eq. (5) are determined only by ns driving pulses and are obtained from the solution of Eqs. (2) and (3)in the first step. In the 1D and dispersionless limits (a_ω, b_ω, and d_ω are frequency independent) the wave Eq. (5) recovers the wave equation used in previous investigations [12,15].

The procedure for solving the system of Eqs. (2), (3), and (5) is as follows. We start with the fields of driving and probe pulses at the entrance of the medium. The field envelopes, in 2D free space, have a form [20]

$$\mathcal{A}(x,z)=\frac{\mathcal{A}_0}{[1+(2z/b)^2]^{0.25}}\exp\left[-\frac{x^2}{w_0^2[1+(2z/b)^2]}+i\varphi\right],$$

$$\varphi=-\frac{1}{2}\arctan\left(\frac{2z}{b}\right)+\frac{2zx^2}{bw_0^2[1+(2z/b)^2]}, \tag{6}$$

where $\mathcal{A}$ stands for $E_q(x,z)$ or $F(x,z,\omega)$, w_0 is the beam waist radius, $b=k_{q,\omega}w_0^2$ represents the confocal parameter, and $\mathcal{A}_0$ is the normalization factor, respectively. The 2D Gaussian beams (6) satisfy the 2D propagation equations for $E_q(x,z)$ or $F(x,z,\omega)$ in free space [Eqs. (3) or (5) with the right-hand sides equal zero]. First, we solved the system of Eqs. (2) by the four-order Runge-Kutta method. Once the solution of Eq. (2) is obtained, the medium states (ρ_{aa}, ρ_{bb}, and ρ_{ab}) are inserted into source terms (right-hand side) of Eqs. (3) and (5). To solve Eqs. (3) and (5) we use the operator splitting method [21]. The advance of electric fields from a transverse x axis at z to a new axis at $z+\Delta z$ is carried out in two steps. In the first step, the diffraction acts alone and in the second step, the nonlinearity acts alone. In the first step, the obtained parabolic equation is solved by using a Crank-Nicholson method [22]. In the second step, the first-order nonlinear differential equation is solved by the second-order Runge-Kutta method. The algorithm is stable and is accurate (in both steps) to second order in step size Δz. This forward propagation continues until the electric-fields $E_q(x,z,\tau)$ and $F(x,z,\omega)$ exit the interaction medium ($z=z_{exit}$). Then, the output spectral or temporal intensities can be obtained by integrating the field intensity over the transverse coordinate

$$I(\omega)\propto\int_{-\infty}^{\infty}|F(x,z_{exit},\omega)|^2dx. \tag{7}$$

Note that, in the case of collinear propagation of waves (in free space or hollow wave-guides) it would be more appropriate to use effective 2D models (3D system with a cylindrical symmetry) than to use 1D or 2D models. The modification of the 2D model presented above to the effective 2D model is straightforward. For this, we simply need to change $x\rightarrow r$, $\partial^2/\partial x^2\rightarrow(1/r)(\partial/\partial r)(r\partial/\partial r)$ (r is the radial coordinate) and use the corresponding Crank-Nicholson technique for cylindrical symmetry [22,23]. We believe that the use of an effective 2D model will not give qualitatively different effects as compared to the 2D model even in the case of collinear propagation of waves. The 3D calculations which take into account the realistic symmetry of solid hydrogen is a difficult task and is exceeding our computation abilities.

III. NUMERICAL RESULTS AND DISCUSSIONS

In this section, we present the numerical results obtained from the solution of the system of Eqs. (2), (3), and (5). The parameters of the fundamental vibrational transition in solid H_2 are [16–18]: $\omega_{ba}=4149.7\ \mathrm{cm}^{-1}$, $T_1=40\ \mu\mathrm{s}$, $T_2=0.1\ \mu\mathrm{s}$, and $N=2.6\times10^{22}\ \mathrm{cm}^{-3}$. We apply two driving

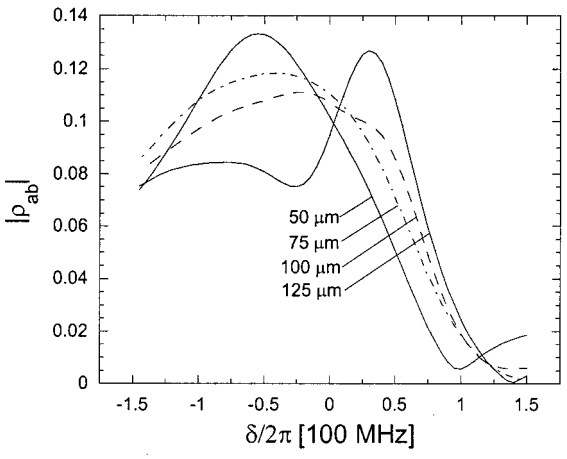

FIG. 2. The absolute value of the on-axis coherence prepared by two nanosecond pulses as a function of the two-photon detuning δ at different propagation distances: 50; 75; 100; and 125 μm ($\theta=0$).

pulses at 355 and 416 nm, both with the same 10 ns pulse width, 200 MW/cm^2 peak intensity, 175 μm beam radius (2 mJ pulse energy), and peak time $\tau=0$. This pumping regime (instead of 738 and 1064 nm as in [15]) permits production of a larger Raman coherence at the same laser intensity and therefore increases the conversion efficiency of the pulse shaping processes [24]. Due to shorter driving wavelengths, we also have a better spatial separation of the generated SFPs from the driving pulses while still keeping the tilt angle θ small. We use the 800-nm, 10-fs probe pulse with the peak intensity 200 MW/cm^2 and the beam radius 60 μm (0.2 nJ pulse energy) to beat with the Raman coherence. The peak time of the probe pulse $\tau_{pr}=21.5$ fs is chosen for the generation of symmetric triplet of SFPs (see Fig. 5 and discussion below). The coefficients a_l, b_l, and d_l ($l=q,\omega$) are taken from the calculations for parahydrogen [11]. We choose the Raman detuning $\delta=-50$ MHz, at which the conditions for the adiabatic coherence preparation are satisfied and a large value of $|\rho_{ab}|$ can be achieved [11]. We note that the key point for successful generation of SFPs is that the probe pulse should be directed along the wave vector of the generated Raman coherence. In our paper, the wave-vector $\vec{k}_m=\vec{k}_0-\vec{k}_{-1}$ is calculated at the entrance of the medium and determines the propagation direction of the probe pulse (z axis). Besides, to achieve the best conversion efficiency, the Raman coherence should not be changed substantially across the probe pulse beam radius. This can be achieved by optimizing the ratio between the beam radius of the driving and probe pulses. In our calculations this ratio is $\sim 3:1$. Also, for the chosen values of laser intensities, the Kerr effect is small and is neglected.

We start our discussion with the coherence prepared by two ns pulses. In Fig. 2, we plot the absolute value of the on-axis Raman coherence $|\rho_{ab}|$ as a function of the two-photon detuning δ at different propagation distances z. The tilt angle between driving pulses $\theta=0$. The calculations show that for the first few tens micrometers of the propagation distance the coherence is a symmetric function of δ (with a maximum at $\delta\simeq 0$). With increasing z, the coherence decreases and becomes an asymmetric function of δ. The maximum value of $|\rho_{ab}|$ is larger than 0.1 and can be achieved over a wide range of z at the Raman detuning $\delta\simeq -50$ MHz. The spatial profile of coherence (not shown here) repeats well the profile of driving pulses.

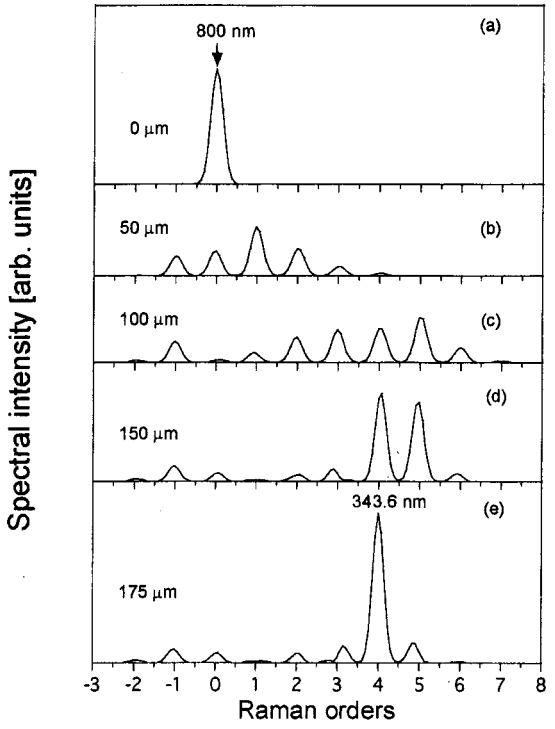

FIG. 3. The spectrum of the femtosecond probe pulse at different propagation distances 0 (a), 50 (b), 100 (c), 150 (d), and 175 (e) μm, respectively. The tilt angle between driving pulses $\theta=5$ mrad ($\alpha\simeq 29$ mrad).

Next, we consider the "beating" of the fs probe pulse with the prepared coherence. In Fig. 3, we present the spectrum of the fs probe pulse at the different propagation distances 0, 50, 100, 150, and 175 μm. The tilt angle between driving pulses $\theta=5$ mrad ($\alpha\simeq 29$ mrad). With increasing propagation distance, the energy of the central component (800 nm) is transferred to both the Stokes and anti-Stokes sides and the number of Raman sidebands gradually increases. At $z\simeq 100$ μm, the central component is almost depleted. At this optimum interaction length the spectrum represents a quasicontinuous broadband which ranges from ~ 2.4 μm to ~ 240 nm. This regime corresponds to the generation of the shortest subfemtosecond pulse in time domain (see Fig. 5). For further increasing interaction length the laser energy continues to transfer to higher anti-Stokes orders. At 175 μm we observed that most of the laser power concentrates on the fourth Raman sideband (343.6 nm). This sideband repeats very well the spectral shape of the probe pulse at the entrance of the medium. This regime can be used for wavelength conversion of the fs probe pulse (see Fig. 6). Within 200 μm interaction length, we observe a very well-preserved Gaussian beam profile for sidebands generated by the probe fs pulse. These sidebands are generated collinearly and are not phase locked (see Fig. 4). The regime, when most

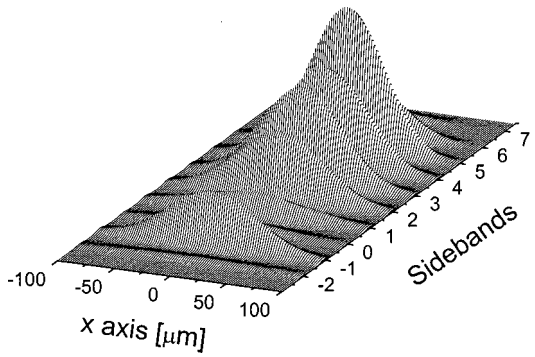

FIG. 4. The spatial profile of sidebands generated by the probe pulse at 100 μm.

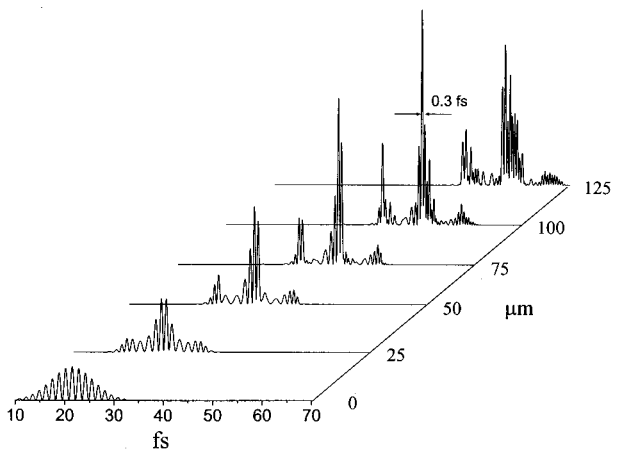

FIG. 5. The temporal profile of the probe pulse at different propagation distances 0, 25, 50, 75, 100, and 125 μm, respectively.

of the laser power is converted into a single sideband can be explained qualitatively in terms of phase matching. The phase matching condition for qth Raman sideband propagating along the wave-vector $\vec{k}_m$ is (see Appendix)

$$\Delta_q + \kappa_q = 0, \tag{8}$$

where

$$\Delta_q = q(k_m - k_m^0) \simeq q(1 - \cos\theta)(k_0 k_{-1}/k_m^0) \tag{9}$$

is the geometrical phase mismatch due to finite angle θ ($\Delta_q = 0$ when $\theta = 0$); $\vec{k}_m = \vec{k}_0 - \vec{k}_{-1}$; $k_m^0 = k_0 - k_{-1} = \omega_m/c$; and κ_q is the sum of molecular phase mismatch and the mismatch due to prepared coherence. Equations (8) and (9) indicate that the phase matching can be achieved for negative κ_q, finite angle θ, and "selected" Raman sideband q^*. In this regime the energy transfer to q^* sideband is most efficient. We have changed tilt angle θ every 2.5 mrad and have observed that when $\theta = 15$ mrad, the selective phase matching occurs for the fifth Raman sideband (300.7 nm). This also indicates that as a function of q, the phase mismatch $-\kappa_q$ changes faster than q. We have evaluated numerically the total phase mismatch ($\Delta_q + \kappa_q$) as a function of q (at $\theta = 5$ mrad). This function changes the sign (from "minus" to "plus") around the fourth sideband and is in good agreement with our qualitative analysis.

The broad and quasicontinuous Raman spectrum can be used for subfemtosecond pulse generation. In Fig. 5, we plot the temporal profile of the probe pulse at different propagation distances 0, 25, 50, 75, 100, and 125 μm. With increasing interaction distance, the input Gaussian pulse gradually reshapes to a clear triplet of subcycle pulses separated by Raman period $T_m = 2\pi/\omega_m \simeq 8$ fs. The peak intensity of the central pulse rapidly increases while its durations decreases with propagation distance. At 100 μm [the broadest and quasicontinuous spectrum in Fig. 3(c)] the central pulse has the shortest pulse duration $\simeq 0.3$ fs and the highest peak intensity (6.5 times higher as compared to the input pulse). Besides, this central subfemtosecond pulse represents a half-cycle pulse. During the propagation one can observe a clear delay of pulse. For 125 μm distance, the delay in local time is $\tau_{del} \simeq 40$ fs. This time delay is in very good agreement with our estimation $\tau_{del} = z/v$ (v is the effective group velocity [15]). We have changed the tilt angle θ every 2.5 mrad to find an optimum regime for subfemtosecond pulse generation. The results show that for $0 \leqslant \theta \leqslant 5$ mrad the peak intensity and the duration of generated SFPs remain nearly unchanged. For $\theta \geqslant 7.5$ mrad the peak intensity gradually decrease, however the pulse duration sharply increase (~ 0.8 fs, single-cycle pulse). Therefore, for generation and detection of the shortest subfemtosecond pulse the optimum tilt angle θ is $\simeq 5$ mrad. At this angle the spatial separation of the probe from the driving pulses $\simeq 14$ mm (after 0.5 m free propagation). We note that the temporal profile of the generated SFPs is sensitive to the peak time τ_{pr}. A gradual increase of τ_{pr} leads to a periodic change (with the period T_m) of the time profile from the symmetric triplet to a doublet of SFPs [15]. This behavior is determined by the dependence of pulse compression on timing of the probe pulse with respect to the molecular oscillation. We note that pulse timing is not an issue when the probe pulse is much longer than the molecular period. In this regime we expect compression of a long pulse train, or conversion into a single high-order Raman sideband, much in the same way as described above. On the contrary, when the pulse length becomes comparable to the molecular period, control of pulse timing becomes crucial for frequency conversion and pulse compression. There are two known mechanisms for the pulse compression. The first one is the generation of a broad frequency-modulation spectrum with the temporal compression by the GVD [8,11,25]. The second one is the direct pulse compression by the molecular oscillations [12,15]. Both mechanisms are included in our numerical model. However, the identification of these mechanisms requires thorough analysis and is out of the scope of this paper.

We turn to discuss the selective phase-matching regime, when most of the laser power is converted to a single high-order Raman sideband [situation of Fig. 3(e)]. This situation corresponds to the wavelength conversion of the fs probe pulse from IR to UV region. Without additional processing, this conversion is not perfect, i.e., the temporal profile of the output pulse is different from the input one. However, since the spectral shape of the phase-matched sideband is very close to the shape of the input probe pulse, this distortion can

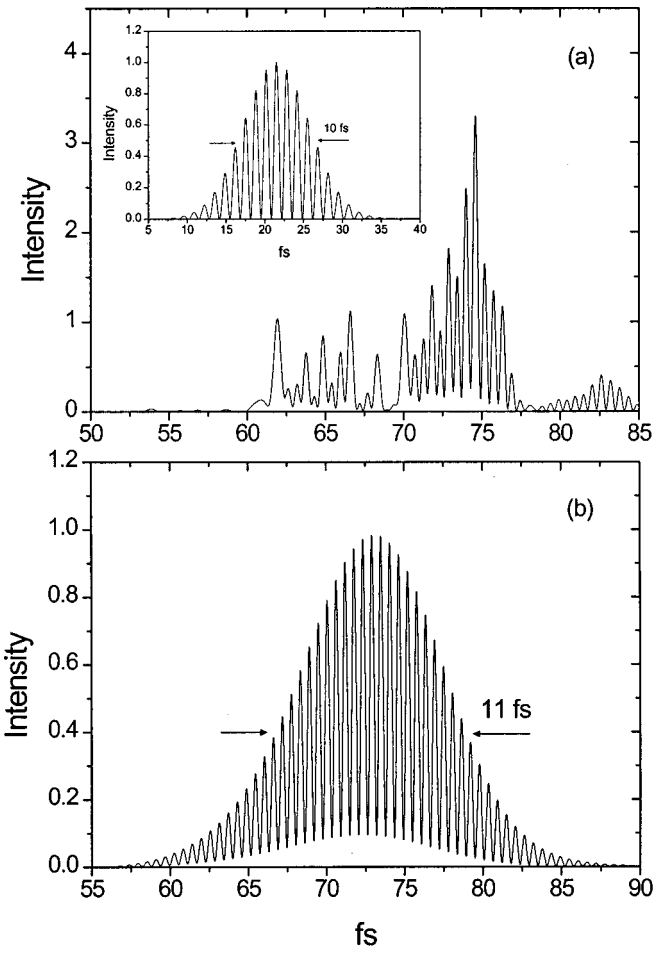

FIG. 6. The temporal profile of the wavelength-converted pulse before (a) and after (b) pulse shaping. The inset (a) shows the profile of the input pulse.

be easily removed. For example, by cutting off small, redundant frequency components in both sides of the phase-matched Raman sideband we can get nearly perfect Gaussian pulse with almost the same pulse width as the input pulse. Figure 6 shows the temporal profiles of the wavelength-converted pulse before (a) and after (b) this simple processing. For comparison the inset in Fig. 6(a) shows the profile of input pulse. Our calculations show that, for the case $\theta = 5$ mrad and 175 μm interaction medium we can convert 800 nm, 10 fs pulse to 343 nm, 11 fs pulse. When the $\theta = 15$ mrad, with the same interaction medium we can convert the same input to 300.7 nm, 11 fs pulse. We note that the integrated intensities in Figs. 6(a) and 6(b) do not go to zero for each oscillation. This is due to small shifts of the time profiles at different positions of the beam radius. The frequency up conversion has been investigated in Refs. [26,27]. In these papers, the conversion is implemented on the first anti-Stokes sideband. Our calculations predict the frequency up conversion on a single high-order Raman sideband.

It is important to note that for both regimes, the subfemtosecond pulse generation and the laser-wavelength conversion, the energy conversion efficiency is larger than unity. In Fig. 7, we plot the energy (normalized to the energy of the input probe pulse) of the pulse triplet and the central pulse of Fig. 5 against the propagation distance. As seen, for an interaction medium longer than 90 μm, the energy conversion efficiency of both the central pulse and the pulse triplet are larger than unity. This is a result of the energy transfer from the driving fields to the probe field via the beating process. The efficiency of the subfemtosecond pulse generation [situation of Fig. 3(c)] is 1.17. The efficiency of the wavelength conversion [situation of Fig. 3(e)] before and after pulse shaping is 1.7 and 1.2, respectively. Our calculations for the probe pulse with the peak intensity one order lower (20 MW/cm^2) show results which are nearly identical to the ones presented above.

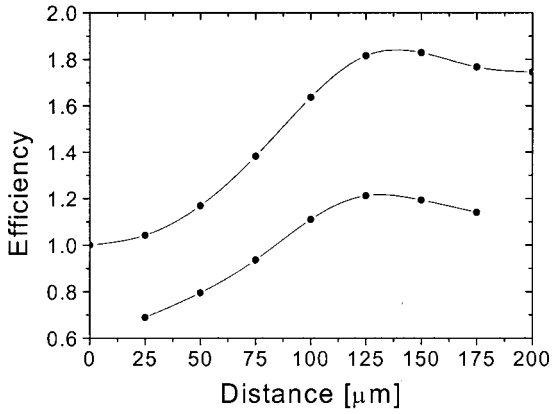

FIG. 7. The energy conversion efficiencies of the pulse triplet (upper curve) and the central pulse (lower curve) as a function of the propagation distance ($\theta = 5$ mrad).

IV. CONCLUSION

In conclusion, we have presented 2D numerical model for the interaction of a fs probe pulse with a Raman medium excited by two ns laser pulses. Numerical results show that by optimizing the tilt angle between the two driving pulses and the interaction length, the power of the probe pulse can be converted either into a quasicontinuous broadband spectrum or into a single high-order sideband. The first regime can be used for generation of subfemtosecond pulses as short as 0.3 fs. The second regime can be used for efficient frequency up conversion of a 10-fs probe pulse from 800 to 343 nm. The use of solid hydrogen with high-molecular density and small interaction length which allows a good overlap of tilted laser beams is an essential point of our technique. The conditions and the setup for the experimental observation of the effects described in this paper could be similar to the situation of our previous experiments [16–18].

ACKNOWLEDGMENTS

A.V.S. wishes to thank David Walker, Deniz Yavuz, and Steve Harris for useful discussions. While at Stanford University, A.V.S. was partially supported by the U.S. Office of Naval Research, the U. S. Army Research Office, and the U. S. Air Force Office of Scientific Research.

APPENDIX

To get insight into the selective phase-matching regime we approximately derive and solve the wave equation for the probe pulse in 1D, dispersionless and SVEA. We assume that the probe pulse propagates along the wave vector of coherence $\vec{k}_m$ (axis z) and express the total electric field of the pulse as follows:

$$F(z,t)=\frac{1}{2}\sum_q F_q(z,t)\exp(ip_q z-\tilde{\omega}_q t)+\text{c.c.}, \quad \text{(A1)}$$

where $\tilde{\omega}_q=\omega_p+q\omega_m$; $p_q=p_0+qk_m$; ω_p, and p_0 are the carrier frequency and the wave vector of the probe pulse, respectively. For finite angle θ, $p_q\neq\tilde{\omega}_q/c$. This formalism is not suitable for changing to local time, however, it enables us to factor out the geometrical phase mismatch terms explicitly. The propagation equation for sideband fields reads

$$\frac{\partial F_q}{\partial z}=\frac{iN\hbar\omega_q}{\epsilon_0 c}[(a\rho_{aa}+b\rho_{bb})F_q+d\rho^*_{ab}F_{q-1}e^{-i\varphi_q}+d\rho_{ab}F_{q+1}e^{i\varphi_{q+1}}]. \quad \text{(A2)}$$

where $\varphi_q=(p_q-p_{q-1}-\omega_m/c)z$. In deriving Eq. (A2) we neglect the contributions $\partial^2F_q/\partial z^2$, $\partial^2F_q/\partial t^2$, and $(1/c)\partial F_q/\partial t$ on the left-hand side. By assuming $\rho_{ab}=\rho_0 e^{i\eta z}$ one can get the equation for $\mathcal{F}_q=F_q e^{i(\Delta_q+q\eta)z}$ as follows:

$$\frac{\partial\mathcal{F}_q}{\partial z}=i(\Delta_q+\kappa_q)\mathcal{F}_q+iB_q(\mathcal{F}_{q+1}+\mathcal{F}_{q-1}), \quad \text{(A3)}$$

where $\Delta_q=q(k_m-k^0_m)$ is the geometrical phase mismatch due to finite angle θ ($\Delta_q=0$ when $\theta=0$); $\vec{k}_m=\vec{k}_0-\vec{k}_{-1}$; $k^0_m=k_0-k_{-1}=\omega_m/c$; $\kappa_q=N\hbar\omega_q(a\rho_{aa}+b\rho_{bb})/\varepsilon_0 c+q\eta$; and $B_q=N\hbar\omega_q d\rho_0/\varepsilon_0 c$. The phase mismatch κ_q is the sum of molecular phase mismatch (first term) and the mismatch due to prepared coherence (second term). The system of coupled Eqs. (A3) can be solved approximately as follows. We assume that, for $q\leqslant -1$ and $q\geqslant q^*+1$, all $\mathcal{F}_q=0$. For $q=0,1,\cdots q^*-2$ the total phase mismatch $\Delta_q+\kappa_q$ are large, so that the derivative of $\mathcal{F}_q$ in the left-hand side of Eq. (A3) can be neglected. Then we obtain

$$\mathcal{F}_{q+1}=-(\Delta_q+\kappa_q)\mathcal{F}_q/B_q-\mathcal{F}_{q-1}. \quad \text{(A4)}$$

Each field amplitude $\mathcal{F}_q$ ($q=1,2,\cdots q^*-1$) can consecutively be expressed via initial $\mathcal{F}_0$ ($\mathcal{F}_{-1}=0$).

$$\mathcal{F}_1=-(\Delta_0+\kappa_0)\mathcal{F}_0/B_0,$$

$$\mathcal{F}_2=-(\Delta_1+\kappa_1)\mathcal{F}_1/B_1-\mathcal{F}_0,$$

$$\cdots,$$

$$\mathcal{F}_{q^*-1}=-(\Delta_{q^*-2}+\kappa_{q^*-2})\mathcal{F}_{q^*-2}/B_{q^*-2}-\mathcal{F}_{q^*-3}.$$

For $q=q^*$, the total phase mismatch is small and the derivative of $\mathcal{F}_{q^*}$ in the left-hand side of Eq. (A3) cannot be neglected. In this case the solution for $\mathcal{F}_{q^*}$ has a form ($\mathcal{F}_{q^*+1}=0$).

$$\mathcal{F}_{q^*}=2iB_{q^*}\mathcal{F}_{q^*-1}\exp[-i(\Delta_{q^*}+\kappa_{q^*})z/2]\times\frac{\sin[(\Delta_{q^*}+\kappa_{q^*})z/2]}{(\Delta_{q^*}+\kappa_{q^*})}. \quad \text{(A5)}$$

The solution (A5) contains a standard phase-matching function $[\sin(x)/x]$ which leads to the condition (8) in the text.

[1] T. Brabec and F. Krausz, Rev. Mod. Phys. **72**, 545 (2000).

[2] P. Salières, A. L'Huillier, P. Antoine, and M. Lewenstein, Adv. At., Mol., Opt. Phys. **41**, 83 (1999).

[3] P.B. Corkum, N.H. Burnett, and M.Y. Ivanov, Opt. Lett. **19**, 1870 (1994); P. Antoine, A. L'Huillier, and M. Lewenstein, Phys. Rev. Lett. **77**, 1234 (1996); K.J. Schafer and K.C. Kulander, *ibid.* **78**, 638 (1997); A. Scrinzi, M. Geissler, and T. Brabec, *ibid.* **86**, 412 (2001); R. Bartels, S. Backus, E. Zeek, L. Misoguti, G. Vdovin, I.P. Christov, M.M. Murnane, and H.C. Kapteyn, Nature (London) **406**, 164 (2000).

[4] M. Drescher, M. Hentschel, R. Kienberger, G. Tempea, C. Spielmann, G.A. Reider, P.B. Corkum, and F. Krausz, Science **291**, 1923 (2001).

[5] P.M. Paul, E.S. Toma, P. Breger, G. Mullot, F. Augé, Ph. Balcou, H.G. Muller, and P. Agostine, Science **292**, 1689 (2001).

[6] S. Yoshikawa and T. Imasaka, Opt. Commun. **96**, 94 (1993).

[7] A.E. Kaplan, Phys. Rev. Lett. **73**, 1243 (1994).

[8] S.E. Harris and A.V. Sokolov, Phys. Rev. Lett. **81**, 2894 (1998); Phys. Rev. A **55**, R4019 (1997).

[9] A. Nazarkin and G. Korn, Phys. Rev. A **58**, R61 (1998); A. Nazarkin, G. Korn, M. Wittmann, and T. Elsaesser, Phys. Rev. Lett. **83**, 2560 (1999).

[10] E.M. Belenov and A.V. Nazarkin, Pis'ma Zh. Éksp. Teor. Fiz. **51**, 252 (1990) [JETP Lett. **51**, 288 (1990)]; E.M. Belenov, A.V. Nazarkin, and I.P. Prokopovich, *ibid.* **55**, 223 (1992) [*ibid.* **55**, 218 (1992)].

[11] Fam Le Kien, J.Q. Liang, M. Katsuragawa, K. Ohtsuki, K. Hakuta, and A.V. Sokolov, Phys. Rev. A **60**, 1562 (1999).

[12] V.P. Kalosha and J. Herrmann, Phys. Rev. Lett. **85**, 1226 (2000).

[13] V.P. Kalosha and J. Herrmann, Phys. Rev. Lett. **83**, 544 (1999).

[14] R.R. Jones, D. You, and P.H. Bucksbaum, Phys. Rev. Lett. **70**, 1236 (1993).

[15] Fam Le Kien, Nguyen Hong Shon, and K. Hakuta, Phys. Rev. A **64**, 051803(R) (2001).

[16] K. Hakuta, M. Suzuki, M. Katsuragawa, and J.Z. Li, Phys. Rev. Lett. **79**, 209 (1997).

[17] J.Q. Liang, M. Katsuragawa, Fam Le Kien, and K. Hakuta, Phys. Rev. Lett. **85**, 2474 (2000).

[18] J.Z. Li, M. Katsuragawa, M. Suzuki, and K. Hakuta, Phys. Rev. A **58**, R58 (1998); J. Z. Li, M. Suzuki, M. Katsuragawa, and K. Hakuta (unpublished).

[19] A.V. Sokolov, D.R. Walker, D.D. Yavuz, G.Y. Yin, and S.E. Harris, Phys. Rev. Lett. **85**, 562 (2000).

[20] A. E. Siegman, *Lasers* (Cambridge University, Cambridge, England, 1986), Chap. 16.

[21] W. H. Press, A. A. Teukolsky, W. T. Vetterling, and B. P. Flannery, *Numerical Recipes in Fortran*, 2nd ed. (Cambridge University, Cambridge, England, 1992), Chap. 19.

[22] G. D. Smith, *Numerical Solution of Partial Differential Equations. Finite Difference Method* (Oxford University, New York, 1985), Chap. 2.

[23] More detailed description of the effective 2D propagation model for HHG problem can be found, for example, in E. Priori, G. Cerullo, M. Nisoli, S. Stagira, S. De Silvestri, P. Villoresi, L. Poletto, P. Ceccherini, C. Altucci, R. Bruzzese, and C. de Lisio, Phys. Rev. A **61**, 063801 (2000); Nguyen Hong Shon, A. Suda, Y. Tamaki, and K. Midorikawa, *ibid.* **63**, 063806 (2001).

[24] This is due to dispersion and can be anticipated from the explicit expressions for coupling coefficients a_q, b_q, and d_q given in Ref. [11]. Neglecting ω_a and ω_b as compared to ω_j, one gets a_q, b_q, and $d_q \sim (\omega_j^2 - \omega_q^2)^{-1} \sim (1 + \omega_q^2/\omega_j^2)$. Therefore, for a shorter driving wavelength, the coupling constants are larger, which leads to a large Raman coherence and a more efficient nonlinear conversion.

[25] A.V. Sokolov, Opt. Lett. **24**, 1248 (1999); A.V. Sokolov, D.D. Yavuz, and S.E. Harris, *ibid.* **24**, 557 (1999).

[26] M. Jain, H. Xia, G.Y. Yin, A.J. Merriam, and S.E. Harris, Phys. Rev. Lett. **77**, 4326 (1996).

[27] A.V. Sokolov, S.J. Sharpe, M. Shverdin, D.R. Walker, D.D. Yavuz, G.Y. Yin, and S.E. Harris, Opt. Lett. **26**, 728 (2001).